International Journal of Thermophysics, Vol. 24, No. 4, July 2003 (© 2003)

Density Determination of Liquid Copper, Nickel, and Their Alloys

J. Brillo[1, 2] **and I. Egry**[1]

Received November 26, 2002

A method for the determination of the density of electromagnetically levitated metallic liquids has been developed. This method employs an enlarged beam of parallel laser light to produce a shadow image of the sample. The shadow is recorded by a digital CCD-camera, and the images are analyzed using an edge detection algorithm. The circumference is fitted by Legendre polynomials that can be used for calculations of the volume of the sample. The method has been tested successfully on various alloys of copper-nickel (Ni_xCu_y), as well as on the pure elements, Cu and Ni. Densities were measured for each sample at different temperatures below and above the melting point, and a linear behavior was observed. At the melting point the densities for copper and nickel were 7.9 and 7.93 $g \cdot cm^{-3}$, respectively. For $T = 1270°C$ liquid copper has a density of 7.75 $g \cdot cm^{-3}$ which strongly increases up to roughly 8.1 $g \cdot cm^{-3}$ if a small amount (10–40 at.%) of nickel is added to the system. For nickel concentrations larger than 50 at.% the density remains nearly constant.

KEY WORDS: alloy; copper; density; electromagnetic levitation; nickel; thermal expansion; thermophysical properties; undercooling.

1. INTRODUCTION

Thermophysical properties of undercooled molten metals such as density, electrical conductivity, surface tension, viscosity, etc. are of particular interest as they play an important role in understanding and defining the thermodynamic state of the system. For undercooled liquids it is a crucial point that these properties can be measured without touching the sample. Therefore, measurement of the thermodynamic properties of undercooled

[1] Deutsches Zentrum für Luft- und Raumfahrt, Institut für Raumsimulation, D-51170 Köln, Germany.
[2] To whom correspondence should be addressed. E-mail: Juergen.Brillo@dlr.de

0195-928X/03/0700-1155/0 © 2003 Plenum Publishing Corporation

liquid samples is often a technical challenge. The technique of electromagnetic levitation (EML) offers a convenient platform on which containerless measurements can be carried out. A comprehensive overview of EML is given in Ref. 1.

In the past density measurements of liquid metals have been carried out on the copper nickel system Ni_xCu_y using EML [2–4], using the so called maximum bubble pressure technique [5] and recently [6] using high temperature electrostatic levitation (HTESL) [7]. However, major differences in these results are common and, therefore, no reliable data are available until now. Furthermore, there are few studies reported on any density measurements. The reason for this is probably that neither a technique that delivers results with the required accuracy nor any reliable theoretical model exists. In this work we describe in detail a new optical method employing EML and present data obtained for the copper-nickel system (Ni_xCu_y). We use Ni_xCu_y as an example to test the new method for the following reasons: data from the literature are available for this system. From a chemical point of view it is a rather simple system as copper and nickel are totally miscible at all temperatures as well as in all stoichiometric ratios [8]. As the vapor pressure is considerably low, the system does not show any pronounced evaporation near the melting point, so that the loss of mass and the change in chemical composition are negligible. Undercooling of Ni_xCu_y can also be routinely achieved. Furthermore, the alloy Ni-44 at.%Cu is known as constantan and is used in various technical applications [9].

2. EXPERIMENTAL SETUP

Experiments were carried out in a vacuum chamber containing a water-cooled coil for the electromagnetic levitation experiment. At the beginning of each experiment, the sample is located in the middle of the coil and the chamber is filled with 800 to 900 mbar argon. If a current of of some 100 A at ≈ 250 kHz is applied to the coil, electromagnetic forces lift the sample. At the same time, currents that are induced inside the sample start heating it. Depending on the material and the available power, a levitated sample can reach temperatures up to $T \approx 2000$°C. Cooling is performed by exposing the droplet to a laminar flow of argon gas. The gas is admitted via a small ceramic tube that is located at the bottom side of the sample. For a more detailed description of the levitation process, see Ref. 10.

For measuring the density, i.e., the volume of the sample, it is of particular importance that the sample is fully visible from the side. We therefore designed a coil that assured that none of the edges of the sample were hidden by the windings of the coil.

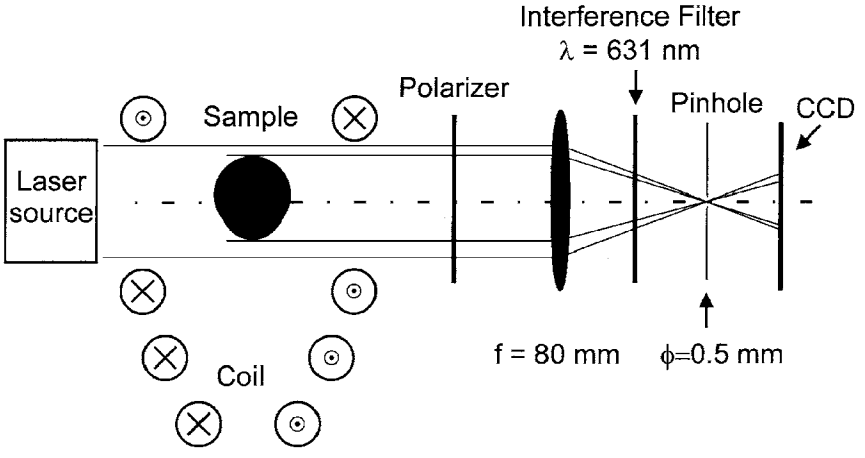

Fig. 1. Schematic diagram of the optical setup.

Figure 1 shows a schematic drawing of the optical setup. A polarized laser beam is produced by a light source (HeNe) equipped with a spatial filter, a beam expander, and a collimator. The light is propagated to the sample from the rear. The collimator of the laser objective is adjusted by means of a shear plate condenser so that the laser beam is parallel. The diameter of the spot is 25 mm. As the laser beam hits the sample and the two windows of the chamber, a major part of the light is deflected due to scattering and diffraction processes. These nonparallel components must be removed in order to obtain a sharp shadow graph image that is free of interferences and diffraction patterns. This task is performed by the lens ($f = 80$ mm) and the pinhole ($\phi = 0.5$ mm) acting together as an optical Fourier filter. In order to vary the intensity of the light, a polarization filter is added to the setup. The interference filter finally removes contributions due to the sample's thermal radiation.

The shadow image then is recorded by means of a digital CCD camera (Ikegami SKC 131) and fed into a computer. The resolution of the camera is 1024×1000 pixels. The camera is operated at a frame rate of $12\ s^{-1}$ with a shutter time of 10^{-3} s. An example of an image of a levitated droplet is shown in Fig. 2.

The images are analyzed in real time by an edge detection algorithm. As described below, the algorithm applies the spatial derivative operator $\|\partial/\partial x\| + \|\partial/\partial y\|$ to the image that detects the edge of the sample.

Let $\{\vec{x}_{\text{Profile}}\}$ be a profile line accross the edge and $\|\partial/\partial\vec{x}\, I(\vec{x}_{\text{Edge}})\|$ be the derivative of the intensity I at $\vec{x}_{\text{Edge}} \in \{\vec{x}_{\text{Profile}}\}$, then a pixel at point $\vec{x}_{\text{Edge}} = (x, y)$ is defined to be an edge pixel if $\|\partial/\partial\vec{x}\, I(\vec{x}_{\text{Edge}})\|$ is larger than

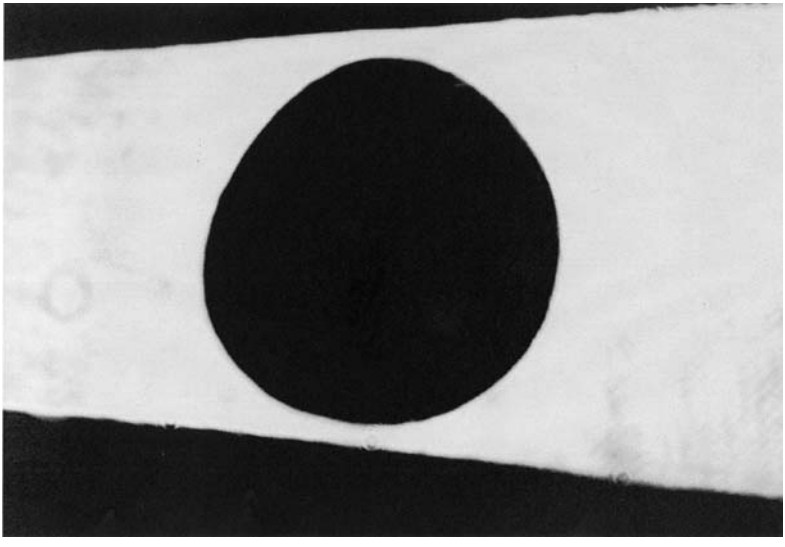

Fig. 2. Shadow graph image of a levitated copper sample at $T \approx 1230°C$. The dark regions at the top and bottom of the figure represent the shadow of the levitation coil.

a fixed threshold and if it is a local maximum. For the subsequent mathematical treatment, the edge points $\vec{x}_{\text{Edge}}$ are conveniently expressed in polar coordinates with respect to the approximate drop center (x_0, y_0). In other words,

$$\vec{x}_{\text{Edge}} \longrightarrow R(\varphi) \tag{1}$$

with R being the radius and φ the polar angle. In EML, however, the surface of the droplet is undergoing oscillations. Each frame, therefore, shows a droplet that is slightly distorted from its ideal equilibrium shape. As long as the amplitudes of these oscillations are comparatively small with respect to the average diameter of the sample, the equilibrium shape can be obtained by averaging $R(\varphi)$ over a number of frames larger than 1000.

We then fit Legendre polynomials of order $\leqslant 6$ to the averaged edge curve $\langle R(\varphi) \rangle$.

$$\langle R(\varphi) \rangle = \sum_{i=0}^{6} a_i P_i(\cos(\varphi)) \tag{2}$$

with P_i being the ith Legendre polynomial.

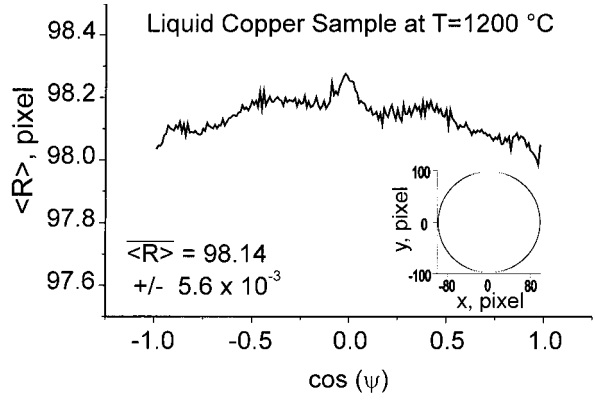

Fig. 3. Average of 1000 frames showing the radius of a levitated copper sample at $T \approx 1200°C$ from the top as a function of the azimuthal angle ψ. The inset shows the same data in cartesian coordinates.

The volume is calculated by the following integral, provided the equilibrium shape of the sample is axisymmetric:

$$V_{\text{Pixel}} = \tfrac{2}{3}\pi \int_0^{\pi} \langle R(\varphi)\rangle^3 \sin\varphi \, d\varphi \tag{3}$$

In Eq. (3), V_{Pixel} is the volume in pixel^3. In order to verify the assumption of axisymmetry, 1000 frames of a liquid copper sample at 1200°C were recorded from the top. As can be seen from Fig. 3, the averaged edge curve $\langle R\rangle$ does not vary much with the azimuthal angle ψ. In fact, the relative deviation is only 5.7×10^{-3}%. In order to calculate the real volume V_{Real} in cm^3, it is necessary to calibrate the system by determining the factor q in $V_{\text{Real}} = qV_{\text{Pixel}}$.

Calibration, however, is crucial as it is required for accurate measurements. In a small temperature range of only 10 K, typical volume changes are approximately 0.1%. For a typical calibration sphere ($\phi = 3$ to 5 mm), this means that deviations are assumed to be less than 30 µm [2]. This is a condition that can easily be fulfilled by balls that are used in bearings as these are manufactured with a tolerance in diameter of 0.5 to 10 µm [11]. In our experiment, we use such balls made by SKF with four different diameters ranging from $\phi = 4.00$ mm up to $\phi = 6.35$ mm. Typical values for q are between 3.0 and 3.1×10^{-9} cm^3.

The temperature of the sample is recorded by means of an infrared pyrometer directed towards the sample from the top. For each sample, the

liquidus temperature T_L was taken from Ref. 8. The sample temperature T was obtained from calibrating the output signal T_P of the pyrometer by using the following approximation derived from Wien's law:

$$\frac{1}{T}-\frac{1}{T_P}=\frac{1}{T_L}-\frac{1}{T_{L,P}} \tag{4}$$

In Eq. (4), $T_{L,P}$ is the pyrometer signal at the liquidus. Equation (4) is valid, if the emissivity $\epsilon(T)$ remains constant over the experimentally scanned range of temperature. This is the case for most materials; see Ref. 12.

Ni_xCu_y samples were prepared by simultaneously melting adequate amounts of copper and nickel in an arc furnace. Samples with nickel weight concentrations ranging from 0% up to 100% were produced. Before the actual experiment took place, each sample was molten in a levitation process so that a homogeneous alloy could form. It was then assumed that, due to segregation, impurities became enriched in the surface region of the droplet. Hence, in a second step, the surface of the solidified sample was polished by mechanical treatment. In order to ensure that the mass of the sample remained constant during the whole time of the experiment, each sample was weighed immediately before and after the measurement. When it turned out that the sample had lost more than $\approx 0.1\%$ of its initial mass, the measurement was omitted.

3. RESULTS AND DISCUSSION

3.1. Pure Elements

The application of this method to solid materials is prone to errors due to possible voids in the sample. In order to prove that the method is providing reliable results for liquid samples, measurements were first done on copper and nickel. Copper and nickel are good candidates because there are reliable data available [2]. In addition, solid samples are not axisymmetric.

Figures 4 and 5 show the density versus temperature for copper and nickel, respectively, and the data are reported in Table I. The data are in good agreement with the data of Ref. 2, and there is even less scatter here. For nickel, however, the data start to strongly scatter at temperatures higher than $T \approx 1500°C$. The reason for this behavior is that, due to the decreased viscosity at elevated temperatures, the sample is starting to perform intense surface oscillations that can no longer be eliminated by averaging. As can be seen from Fig. 5, this effect can be slightly reduced by using lower masses of the sample.

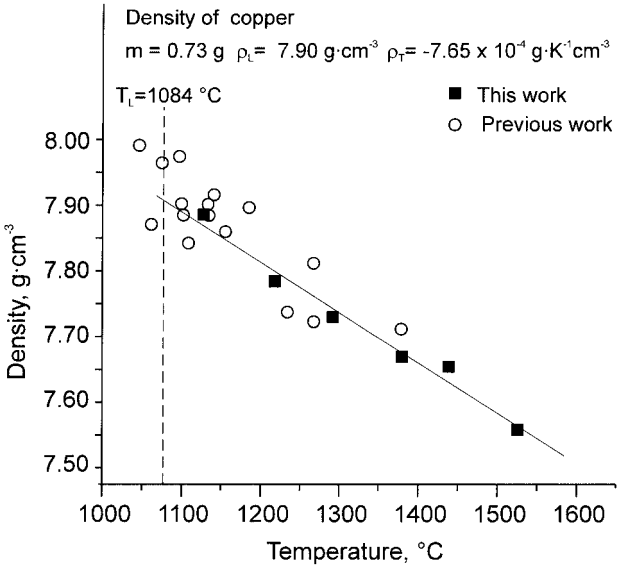

Fig. 4. Density of liquid copper in comparison to data taken from Ref. 2.

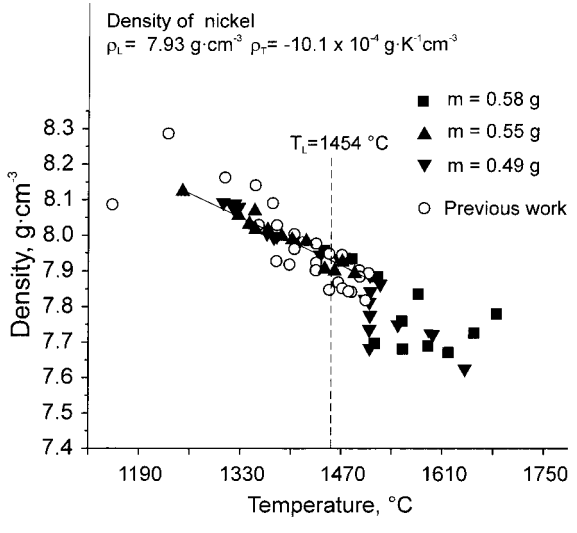

Fig. 5. Density of liquid nickel in comparison to data taken from Ref. 2.

Table I. Experimental Density Data for Nickel and Copper

Nickel				Copper	
T (°C)	ρ (g·cm^{-3})	T (°C)	ρ (g·cm^{-3})	T (°C)	ρ (g·cm^{-3})
1250	8.128	1466	7.932	1127	7.886
1305	8.089	1471	7.926	1217	7.784
1307	8.092	1476	7.941	1291	7.730
1319	8.076	1484	7.933	1379	7.670
1322	8.08	1488	7.893	1438	7.655
1327	8.056	1500	7.824	1525	7.559
1327	8.075	1509	7.733		
1341	8.031	1509	7.810		
1342	8.039	1510	7.680		
1343	8.029	1510	7.772		
1350	8.069	1510	7.885		
1350	8.017	1510	7.839		
1353	8.019	1516	7.696		
1366	7.996	1520	7.884		
1367	8.016	1524	7.860		
1368	8.015	1524	7.860		
1376	7.991	1548	7.746		
1380	7.994	1554	7.758		
1387	7.997	1554	7.680		
1401	7.988	1576	7.835		
1404	7.982	1590	7.689		
1407	7.959	1591	7.726		
1421	7.983	1596	7.718		
1440	7.942	1618	7.670		
1446	7.956	1641	7.622		
1446	7.906	1653	7.725		
1460	7.901	1684	7.779		

From both figures it can be seen that the density ρ is a linear function of temperature T:

$$\rho(T) = \rho_L + \rho_T(T - T_L) \tag{5}$$

where T_L is the temperature at liquidus, ρ_L is the density at $T = T_L$, and ρ_T is the temperature coefficient of the density. The values for the parameters ρ_L and ρ_T are listed in Table IV for copper and nickel, respectively. The values for ρ_L are all within a margin of $\pm 1\%$ indicating good agreement of the data. The values for ρ_T lie within a margin $\approx \pm 12\%$ except for the one that was determined by means of HTSEL, which is significantly lower. The greater differences of the data for ρ_T indicate that a determination of ρ_T is more difficult than a measurement of ρ_L.

Table II. Experimental Density Data for Ni_xCu_y Samples (C_{Ni} = 10 to 40 mass%)

Ni 10 mass%		Ni 20 mass%		Ni 40 mass%	
T (°C)	ρ (g·cm^{-3})	T (°C)	ρ (g·cm^{-3})	T (°C)	ρ (g·cm^{-3})
1059	8.040	1143	8.123	1284	8.087
1089	8.022	1152	8.113	1299	8.101
1139	7.955	1199	8.097	1302	8.074
1151	7.964	1214	8.091	1319	8.058
1153	7.960	1253	8.085	1327	8.047
1170	7.940	1281	8.003	1348	8.038
1172	7.945	1299	7.998	1369	8.021
1180	7.931	1321	7.964	1384	7.983
1196	7.931	1341	7.956	1395	8.014
1216	7.898	1369	7.900	1408	7.970
1257	7.868	1390	7.907	1418	7.990
1279	7.889			1419	7.952
1280	7.854			1420	7.950
1280	7.882			1435	7.923
1302	7.842			1435	7.924
1303	7.817			1442	7.897
				1444	7.887
				1461	7.884
				1461	7.879

Despite the problem occurring for nickel at $T \geqslant 1500$°C, it can be concluded that for the simple systems, copper and nickel, the method proposed in this work is producing results with sufficient reliability. It is therefore justified to move on to more complex systems, i.e., binary alloys.

3.2. Alloys

For each of the alloy samples, density data were recorded at temperatures above and below the liquidus temperature T_L. The data are given in Tables II and III and plotted in Fig. 6. The parameters ρ_L and ρ_T are reported in Table V.

From these parameters, the density at all temperatures and concentrations can be extrapolated. In order to study the concentration dependence of the density, it was calculated at $T = 1272$°C. This temperature was chosen because it lies half way between the melting temperatures of copper and nickel, and because previous data exist for comparison. The results are shown in Fig. 7. Starting with copper, the density increases nearly linearly

Table III. Experimental Density Data for Ni_xCu_y Samples (C_{Ni} = 50 to 90 mass%)

Ni 50 mass%		Ni 70 mass%		Ni 90 mass%	
T (°C)	ρ (g·cm^{-3})	T (°C)	ρ (g·cm^{-3})	T (°C)	ρ (g·cm^{-3})
1228	8.163	1356	8.100	1340	8.037
1238	8.168	1357	8.050	1344	8.048
1250	8.161	1385	8.038	1350	8.019
1268	8.144	1405	8.047	1360	8.031
1294	8.123	1417	8.056	1367	8.014
1340	8.083	1428	8.008	1371	8.018
1366	8.059	1428	8.051	1382	8.026
1393	8.052	1457	7.996	1395	8.011
1410	8.027	1468	7.976	1403	8.004
1437	8.014	1477	7.994	1425	7.976
		1488	7.925	1433	7.947
				1441	7.935
				1453	7.966
				1472	7.907

Table IV. Parameters ρ_L and ρ_T of Pure Nickel and Copper Compared with Literature Data

System	ρ_L (g·cm^{-3})	ρ_T (10^{-4} g·cm^{-3}·K^{-1})	Reference
Ni	7.89	−12	[4]
Ni	7.91	−11.1	[2]
Ni	7.86	−6.73	[6]
Ni	7.93	−10.1	Present work
Cu	8.03	−7.9	[5]
Cu	8.09	−9.4	[3]
Cu	7.92	−8.4	[2]
Cu	7.90	−7.65	Present work

Table V. Parameters ρ_L and ρ_T of Ni_xCu_y Samples

mass% Ni	T_L (°C)	ρ_L (g·cm^{-3})	ρ_T (10^{-4} g·cm^{-3}·K^{-1})
0	1084	7.90	−7.65
10	1136	7.97	−7.95
20	1200	8.09	−9.57
40	1280	8.13	−10.3
50	1320	8.10	−7.72
70	1380	8.06	−9.11
90	1433	7.96	−9.26
100	1454	7.92	−10.1

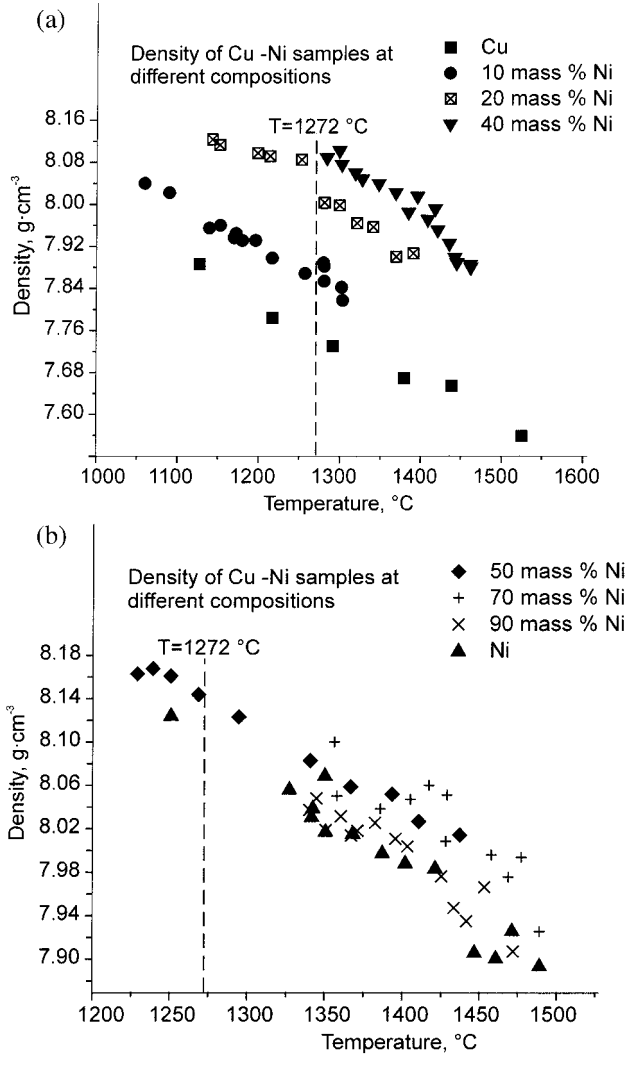

Fig. 6. Density of different Ni_xCu_y samples versus temperature. (a) $C_{Ni} = 0$ to 40 mass%, (b) $C_{Ni} = 50$ to 100 mass%.

from a value of $\approx 7.75\ g \cdot cm^{-3}$ up to ≈ 8.1 to $8.2\ g \cdot cm^{-3}$ as the nickel mass percentage is altered to $\approx 50\%$. On further increase of the nickel concentration, the density values appear to remain more or less constant at this level. A slight decrease might be observed only for nickel concentrations larger than ≈ 80 mass%.

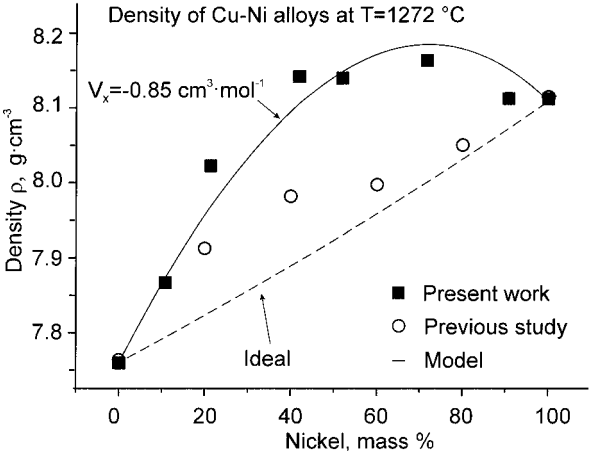

Fig. 7. Density of liquid Ni_xCu_y at $T = 1272°C$ as a function of nickel concentration in comparison to data taken from Ref. 2.

For the investigated alloys, the values of the density in Fig. 7 are significantly higher than the values reported in the earlier work [2], which is almost certainly due to our improved system. The thermal expansion coefficient for the density ρ_T is plotted in Fig. 8 versus the nickel mass percentage. The scatter of the data in this figure is larger than for the values for ρ_L and ρ (1272°C); however, as a general tendency, a steady decrease from $-7.65 \times 10^{-4}\ g \cdot cm^{-3} \cdot K^{-1}$ down to $-10.1 \times 10^{-4}\ g \cdot cm^{-3} \cdot K^{-1}$ is observed.

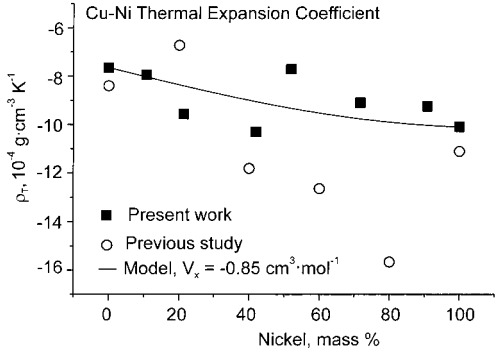

Fig. 8. Thermal expansion coefficient of the density ρ_T versus nickel concentration in comparison to data taken from Ref. 2.

3.3. Interpretation and Model

The density ρ may be expressed as

$$\rho = \frac{C_{Ni} m_{Ni} + C_{Cu} m_{Cu}}{C_{Ni} \frac{m_{Ni}}{\rho_{Ni}} + C_{Cu} \frac{m_{Cu}}{\rho_{Cu}} + V_E} \tag{6}$$

In the above equation, C_{Ni}, C_{Cu} are the atomic concentrations of copper and nickel; $m_{Ni} = 58.7\ \mathrm{g \cdot mol^{-1}}$ and $m_{Cu} = 63.55\ \mathrm{g \cdot mol^{-1}}$ are the corresponding molar masses; and ρ_{Ni}, ρ_{Cu} are the densities of the pure components as taken from Table V. V_E is the excess volume which is the difference between the real volume V and the ideal volume V_{Ideal}, i.e.,

$$V_E = V - V_{Ideal} = V - \left(C_{Ni} \frac{m_{Ni}}{\rho_{Ni}} + C_{Cu} \frac{m_{Cu}}{\rho_{Cu}} \right) \tag{7}$$

In a first approach, we assume the excess volume V_E depends on the concentrations according to

$$V_E = C_{Ni} C_{Cu} V_X \tag{8}$$

with V_X being a type of interaction parameter. If V_X is assumed to be a constant, independent of temperature and concentration, Eq. (6) can be fitted to the experimental data by adjusting V_X as the only parameter; see Fig. 7. The value of V_X obtained from such a fit is $\approx -0.85\ \mathrm{cm^3 \cdot mol^{-1}}$, indicating that the average excess volume is negative. The dashed line in Fig. 7 marks the density with the excess volume V_E in Eq. (6) set to zero, i.e., ideal behavior.

This shows that Eq. (6) describes the density behavior quantitatively and, hence, it is justified to determine the excess volume as a function of the concentration by using the measured values for the density ρ as input to the equation.

The results are shown in Fig. 9 for various temperatures. As is evident, the excess volume depends on temperature only very weakly. At low nickel concentrations, the excess volume strongly decreases until a pronounced minimum of $V_E / V_{Ideal} \approx -3\%$ is reached at $C_{Ni} \approx 40$ mass%.

Equation (6) can also be used in order to derive a formula for ρ_T by simple differentiation:

$$\rho_T = \frac{[C_{Ni} m_{Ni} + C_{Cu} m_{Cu}] \times [C_{Ni} \frac{m_{Ni} \rho_{T,Ni}}{\rho_{Ni}^2} + C_{Cu} \frac{m_{Cu} \rho_{T,Cu}}{\rho_{Cu}^2}]}{[C_{Ni} \frac{m_{Ni}}{\rho_{Ni}} + C_{Cu} \frac{m_{Cu}}{\rho_{Cu}} + C_{Cu} C_{Ni} V_X]^2} \tag{9}$$

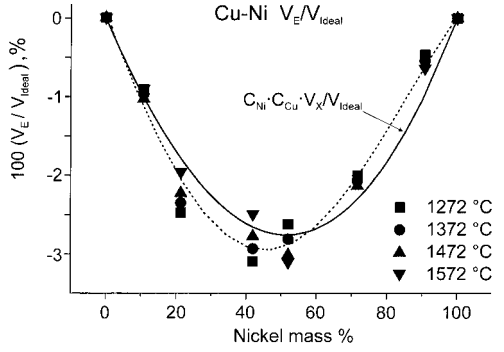

Fig. 9. Excess volume in percent of the ideal volume as calculated from the experimental density data of Ni_xCu_y at various temperatures. The dashed line is a fourth-order polynomial that was fitted to the data for the sake of clarification. The solid line shows Eq. (8) divided by V_{Ideal} for comparison.

In this expression, ρ_{Ni}, ρ_{Cu} are the densities and $\rho_{T,Ni}$ and $\rho_{T,Cu}$ are the thermal expansion coefficients of nickel and copper, respectively. The values for these parameters are taken from Table I. The value for V_X is taken from Fig. 7, and since it is used in Eq. (9) and the temperature dependence of V_X can be neglected (see Fig. 9), there are no additional parameters for fitting. The results are shown as a solid line in Fig. 8, and it turns out that Eq. (9) reproduces the measured data without any fitting.

The density behavior of the Ni_xCu_y alloys presented in this work lead towards the following qualitative explanations. If the concentration of nickel in the Ni_xCu_y melt is low, the nickel atoms might locate themselves into the free volume between the copper atoms which is altering the mass of the sample while its volume is, more or less, constant. The result is not only an increase of the density, as observed in Fig. 7, but also a decrease of the excess volume, as noted in Fig. 9. As soon, however, as nearly all the voids are occupied by nickel atoms, the mass and volume are changing at the same rate keeping the density constant as can be seen again from the data in Fig. 7.

In the framework of such a simple picture, the average distance between the atoms should be smaller in a nickel sample than in a copper sample, which is indeed the case for the crystalline solid material. Although the situation might be very different in the liquid phase, additional support was given just recently as it was shown that there is a kind of fcc structure in the liquid Cu-70 at.%Ni phase, which is maintained upon solidification [13].

For nickel concentrations above and below ≈ 40 mass%, there appears to be a a characteristic change in the physical behavior of the liquid Ni_xCu_y system. This becomes not only evident from the density data from this work but also from measurements of the electrical resistivity [14]. In this study it was observed that for nickel concentrations lower than 40 mass% the temperature dependence of the resistivity followed a quadratic behavior while above 60 mass% the usual linear behavior could be observed. It was, therefore, concluded that at low concentrations, the Ni atoms might also tend to form tiny aggregates leading to local fluctuations in the density while this is not the case at higher concentrations.

4. SUMMARY

Electromagnetic levitation offers an opportunity for contactless measurement of thermophysical properties of undercooled metallic liquids. As for the density, we have developed a technique that, instead of the direct image, records and processes the shadow graph of the sample. This is done in order to minimize problems that originate from the sample's thermal radiation and movements parallel to the optical axis. The method was validated by reproducing the densities and thermal expansion coefficients of pure copper and nickel, and it turned out that the achieved accuracy was higher than in previous studies. We also measured the densities of Ni_xCu_y alloys and discussed the results by means of simple models. In order to get more insight into the microscopic details, the employment of additional experimental techniques such as x-ray diffraction or neutron scattering will be required.

ACKNOWLEDGMENT

The support of this work by the "Deutsche Forschungsgemeinschaft" is gratefully acknowledged.

REFERENCES

1. P. R. Sahm, I. Egry, and T. Volkmann, *Schmelze, Erstarrung, Grenzflächen*. (Friedr. Vieweg und Sohn, Wiesbaden, Braunschweig, 1999).
2. E. Gorges, *Bestimmung der Dichte und Oberflächenspannung von levitierten flüssigen Metallegierungen am Beispiel des Systems Kupfer-Nickel*, Ph.D. thesis (Rheinisch-Westfälische-Technische Hochschule Aachen, 1996).
3. A. E. El-Mehairy and R. G. Ward, *Trans. Met. Soc. AIME* **227**:1226 (1963).
4. S. Y. Shiraishi and R. G. Ward, *Can. Met. Quat.* **3**:117 (1964).
5. A. Saito and S. Watanabe, *Nipp. Kinz. Gakk.* **35**:554 (1971).
6. S. K. Chung, D. B. Thiessen, and W. K. Rhim, *Rev. Sci. Instrum.* **67**:3175 (1996).

7. W. K. Rhim, S. K. Chung, D. Barber, K. F. Man, G. Gutt, A. Rulison, and R. E. Spjut, *Rev. Sci. Instrum.* **64**:2961 (1993).
8. T. B. Massalski, *Binary Alloy Phase Diagram* (American Society for Metals, Materials Park, Ohio, 1986).
9. E. Hornbogen and H. Warlimont, *Metallkunde* (Springer-Verlag, Berlin, Heidelberg, New York, 1991).
10. I. Egry, G. Lohöfer, and S. Sauerland, *Int. J. Thermophys.* **14**:573 (1993).
11. International Organization for Standardization, *Rolling Bearings–Radial Bearings–Tolerances*, ISO 492 (2002).
12. S. Krishnan, G. P. Hansen, R. H. Hauge, and J. L. Margrave, *High Temp. Sci.* **29**:17 (1990).
13. X. Tian, X. Chen, and A. G. Ilinsky, *Sci. in China, Ser. A–Math., Phys., Astronomy* **43**:1301 (2000).
14. T. Richardsen, G. Lohöfer, and I. Egry, *Int. J. Thermophys.* **23**:1207 (2002).